




Article

# Archaeometric Characterisation of Decorated Pottery from the Archaeological Site of Villa dei Quintili (Rome, Italy): Preliminary Study

Michela Ricca <sup>1</sup>, Giuseppe Paladini <sup>2</sup>, Natalia Rovella <sup>1</sup>, Silvestro Antonio Ruffolo <sup>1</sup>,  
Luciana Randazzo <sup>1</sup> , Vincenza Crupi <sup>3</sup>, Barbara Fazio <sup>4</sup>, Domenico Majolino <sup>2</sup> ,  
Valentina Venuti <sup>2</sup> , Giuliana Galli <sup>5</sup> and Mauro Francesco La Russa <sup>1,6,\*</sup>

<sup>1</sup> Dipartimento di Biologia, Ecologia e Scienze della Terra (DiBEST), Università della Calabria, Via Pietro Bucci, 87036 Arcavacata di Rende (CS), Italy; michela.ricca@unical.it (M.R.); natalia.rovella@unical.it (N.R.); silvestro.ruffolo@unical.it (S.A.R.); luciana.randazzo@unical.it (L.R.)

<sup>2</sup> Dipartimento di Scienze Matematiche e Informatiche, Scienze Fisiche e Scienze della Terra, Università degli Studi di Messina, viale F. Stagno d'Alcontres 31, 98166 Messina, Italy; gpaladini@unime.it (G.P.); domenico.majolino@unime.it (D.M.); vvenuti@unime.it (V.V.)

<sup>3</sup> Dipartimento di Scienze chimiche, biologiche, farmaceutiche ed ambientali, Università degli Studi di Messina, viale F. Stagno d'Alcontres 31, 98166 Messina, Italy; vcrupi@unime.it

<sup>4</sup> CNR-IPCF Istituto per i Processi Chimico Fisici, viale F. Stagno d'Alcontres 37, Faro Superiore, I-98158 Messina, Italy; fazio@ipcf.cnr.it

<sup>5</sup> Soprintendenza Speciale per i Beni Archeologici di Roma, Villa dei Quintili, via Appia Nuova 1092, 00197 Roma, Italy; giuliana.galli66@gmail.com

<sup>6</sup> Institute of Atmospheric Sciences and Climate, National Research Council, Via Piero Gobetti, 101, 40129 Bologna, Italy

\* Correspondence: mlarussa@unical.it

Received: 18 February 2019; Accepted: 12 April 2019; Published: 16 April 2019



**Abstract:** This work focused on the study of decorated pottery dated back to the 16th century from the Roman archaeological site of Villa dei Quintili, a monumental complex located in the south-eastern part of Rome (Italy). A minero-petrographic and geochemical study was undertaken to analyse five archaeological samples in order to define textural features and raw materials used for their production, along with the chemical and physical composition of the superficial decorative glazed coatings. For this purpose, different analytical methods were used, such as polarising optical microscope (POM), X-ray diffraction (XRD), micro-Raman spectroscopy, X-Ray fluorescence (XRF), and electron microprobe analysis coupled with energy dispersive spectrometry (EMPA-EDS). The results of such a multidisciplinary approach allowed us to achieve important results crucial to recognise the shards as majolica of the Renaissance period, improving knowledge about manufacturing processes of these renowned painted ceramic artefacts.

**Keywords:** decorative glazed coatings; EMPA-EDS; micro-Raman spectroscopy; pottery; petrography

## 1. Introduction and Archaeological Setting

Starting from the late Middle Ages, Central Europe and the surrounding areas shared a similar ceramic tradition that was in many ways continued over time [1]. It was mainly in the Renaissance period that art and traditions made their mark in pottery, strongly coloured and painted with natural motifs and geometrical patterns. Renowned painted production centres were especially those of the Italian, Austrian, French, Spanish, Portuguese, and Dutch workshops [2].

In Italy and in the whole Mediterranean basin, the vast ceramic production drove its roots thanks to the abundance of clay deposits and the high level of skillfulness of local artisans that was established

over the centuries. Ceramic shards have been found in numerous archaeological excavations in Italy, as in the case of the complex of Villa dei Quintili (Rome, Italy) [3,4].

Villa dei Quintili (Figure 1), located on the Appia Antica road, is one of the most important monumental complexes located in the Roman suburbs, a few kilometres from the centre of Rome [5–8]. The name Quintili was given in the first half of the 19th century (namely in 1828), following the discovery of several *fistulae aquariae* bearing the inscription “Quintilii Condianus et Maximus”. Such inscriptions attest that the Villa was owned by the brothers Quintili, Sesto Quintilio Condiano and Sesto Quintilio Valerio Massimo, descendants of a senatorial family, towards the end of the 2nd century A.D. [8,9]. Extending on an area of approximately 24 ha, the complex includes the residential area, the thermal environments (consisting of *Calidarium*, *Frigidarium*, and *Tepidarium*), a *Viridarium* (a building that was born as a small amphitheatre for gladiatorial games and later replaced by a panoramic garden), the *Xystus* (a straight portico about 300 m long, set up as a garden for walking and jogging), the *Nymphaeum* (a colossal fountain probably representing the original entrance of the Villa), and, finally, the *Basis Villae*, namely the artificial terraces working as the base of the *Urban Villas* [8,10] (Figure 2a). The Villa was in use until the 6th century A.D., becoming the property of several dynasties which introduced continuous changes to the structures. Then, it fell into disuse and was partially ruined [11].

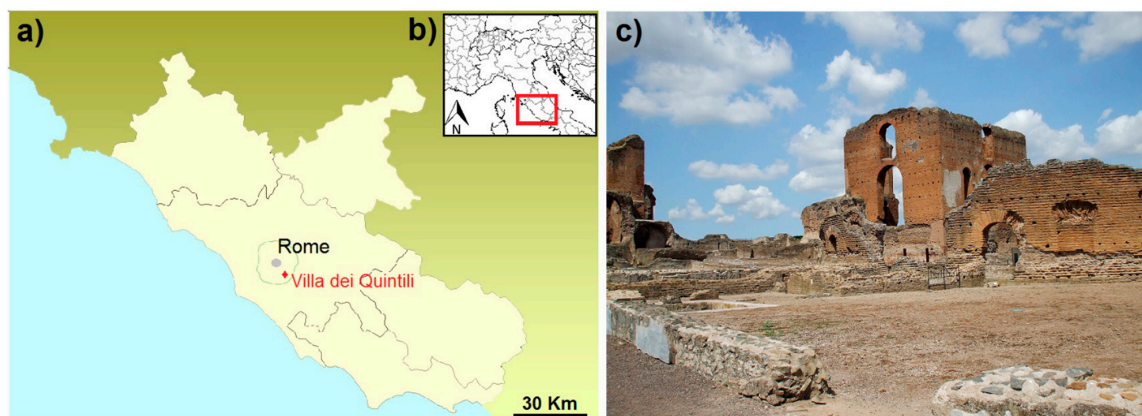


**Figure 1.** Location of Rome, showing the position of Villa dei Quintili (Rome, Italy) in (a) the Lazio region and (b) Italy, and (c) view of some archaeological ruins of Villa dei Quintili.

It was only between the 18th and the 19th centuries A.D. that the first archaeological excavation of the Villa was performed, bringing to light great architectural and sculptural items, testifying the succession of styles that occurred over time in art and technologies. However, due to the significant extent of the monumental complex, much still remains unexcavated and uninvestigated.

In this work, for the first time, ceramic shards with decorative glazed coatings were chosen for archaeometric investigations. Since these potteries are still unexplored from the archaeometric point of view, it is desirable that the results reported here, relative to both the ceramic body and the polychrome glazes, could give an important contribution to the knowledge of painted pottery technology.

Sampling was performed by the archaeologists who have excavated the Villa on behalf of the Archaeological Superintendence of Rome during the archaeological survey campaigns carried out between 1998 and 2004. During the excavations, a lot of pottery fragments (about 30) with decorative glazed coatings were recovered within three different stratigraphic units of the Villa (namely US-3896, US-3235, and US-1229).

On the basis of a first macroscopic classification and of similar properties, all the fragments have been grouped firstly according to the shape, and then considering decoration and colour.

The typology identified are two: (a) Open (plates), and (b) closed (jugs) shapes, decorated respectively with polychrome band decorations (mainly light blue, blue, green, and yellow) on a white background, and with blue and yellow floral decorations on a white background, or rarely in

dark-brown and light blue on a white background. For the present study, five fragments (Figure 2b) were selected considering their state of preservation, distinctive decorative motifs, colours, and shapes. In detail, the samples VQC1 and VQC2 belong to the typology "a" and, on the contrary, VQC3, VQC4, and VQC5 belong to the type "b". From a macroscopic point of view, samples appeared to be intact and well preserved, except for some portions showing a brownish superficial layer, probably due to burial conditions.

The investigation of the fragments was carried out by following a multi-analytical approach, involving the use of geochemical techniques and non-invasive (or minimally invasive) spectroscopic methods [12–15]. Specifically, the minero-petrographic features of the ceramic bodies were evaluated by the use of polarising optical microscope (POM) along with X-Ray diffraction (XRD), while X-Ray fluorescence emission (XRF), micro-Raman spectroscopy, and electron microprobe analysis coupled with energy dispersive spectrometry (EMPA-EDS) were performed in order to analyse the composition of glazes and pigments, respectively used as covering and decoration.

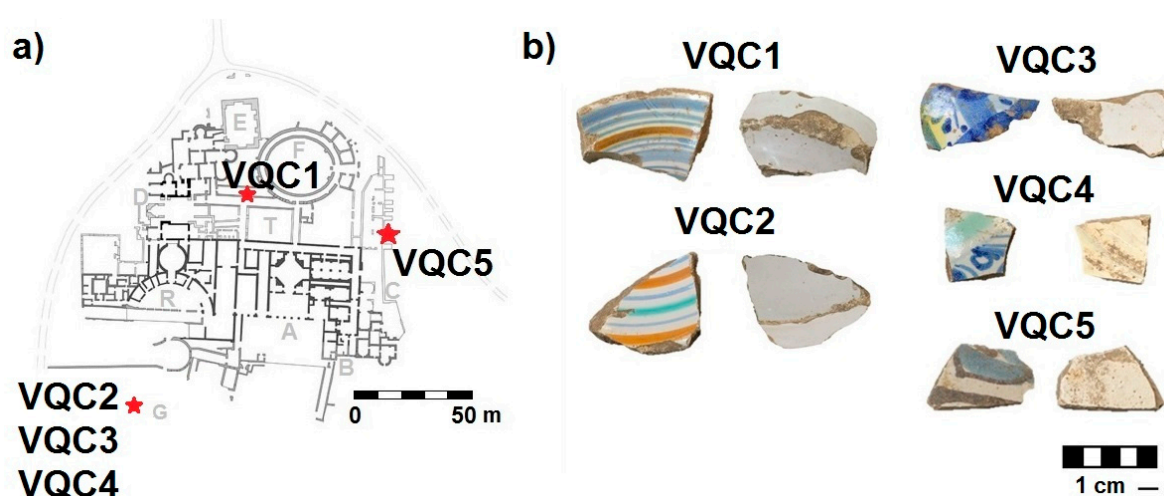


**Figure 2.** (a) Plan of the Villa dei Quintili and details of the sampled areas. Notes: A = representation area; B = private residences; C = Basis Villae; D = Frigidarium; E = Calidarium; F = Ludus-Viridarium; G = great cistern; R = Hippodrome; T = Arcades. (b) Photographs, front and reverse-side, of the analysed fragments.

A list of the examined pottery and brief macroscopic descriptions are summarised in Table 1.

**Table 1.** Macroscopic features of investigated samples together with the recovering area according to Figure 2b.

| Sample | Description  | Recovering Area                  |
|--------|--|----------------------------------|
| VQC1   | Open shape (probably a plate) with polychrome bands decoration on a white background.<br>Predominant colours: light blue, blue, orange         | Corridor of the Ludus-Viridarium |
| VQC2   | Open shape (probably a plate) with polychrome bands decoration on a white background.<br>Predominant colours: green, blue, orange              | Faced with the Great cistern     |
| VQC3   | Closed shape (probably a jug) with polychrome floral decoration on a white background.<br>Predominant colours: light blue, blue, green, yellow | Faced with the Great cistern     |
| VQC4   | Closed shape (probably a jug) with polychrome floral decoration on a white background.<br>Predominant colours: blue, green                     | Faced with the Great cistern     |
| VQC5   | Closed shape (probably a jug) with polychrome floral decoration on a white background.<br>Predominant colours: light blue, dark-brown          | Basis Villae                     |

## 2. Analytical Methods

Archaeometric analyses of the selected pottery fragments were carried out on a representative portion of each sample, considering both the ceramic body and the pigmented surfaces (Figure 2b). Specifically, the analytical techniques applied for a complete characterisation of samples include:

1) Polarising optical microscopy (POM) on thin and stratigraphic sections, in order to determine the petrographic and textural features of painted pottery. Observations were performed using an Axioskope 40 (Axiolab Zeiss) microscope equipped with a digital camera to capture images.

2) X-Ray Powder Diffraction (XRD), which was primarily aimed at individuating the mineralogical phases composing the ceramic bodies. No contamination of the pastes with glaze was possible, because materials were chipped-off exclusively from the bodies of the shards. Each sample was powdered (hand grinding) to pass through a 325 mesh sieve (45  $\mu\text{m}$ ). XRD measurements were obtained by a D8 Advance Bruker X-ray diffractometer with Cu  $K\alpha$  radiation as the X-ray source. The diffractograms were recorded in the  $2\theta$  range of 0–60°. Measuring conditions were set at 40 kV voltage, 30 mA current, 0.02°  $2\theta$  step size, and 3.0 s step time. The EVA software program (DIFFRAC plus EVA) was used to identify the mineral phases in each X-ray powder spectrum, by comparing experimental peaks with PDF2 reference patterns.

3) X-Ray Fluorescence (XRF), for the identification of the elemental constituents of pigments and glazes. XRF measurements were performed by using a portable XRF “alpha 4000” (Innovex-X system) analyser that allowed the detection of various chemical elements having an atomic number (Z) between phosphorus and lead. The apparatus was equipped with a Ta anode X-ray tube excitation source and a high-resolution Si PIN diode detector with an active area of 170 mm<sup>2</sup>. The instrument operated in “soil” mode and two sequential tests were performed on each sample. This configuration allowed us to detect elements from levels of ppm (parts per million). The operating conditions were 40 kV and 7  $\mu\text{A}$  for the first run and 15 kV and 5  $\mu\text{A}$  for the second one, for a total spectrum collection time of 120 s. The two sequential measurements allowed us to detect elements from P to Pb. A Hewlett-Packard iPAQ Pocket PC was used to control the instrument and data storage. The calibration was performed by soil LEAP II and was verified using alloy-certified reference materials produced by Analytical Reference Materials International. The fluorescence signal was collected for about 60 s per run in order to increase the statistics. For all the investigated samples, the lines detected at about 8.15 and 9.34 keV are attributed to the  $L_{\alpha}$  and  $L_{\beta}$  transitions of the Ta anode. When Cu is present, the  $L_{\alpha}$  line of Ta is superimposed to the  $K_{\alpha}$  line of Cu.

4) Micro-Raman spectroscopy, for the characterisation, at molecular scale, of the pigmenting agents and glazed coatings. Micro-Raman spectra were collected, in non-invasive way, by means of a LabRam HR800 Raman confocal Micro-Spectrometer (Horiba-Jobin Yvon) in the back-scattering configuration. The setup is coupled to a He–Ne laser (633 nm), an argon ion laser used to produce the UV line at 364 nm, a solid-state laser at 561 nm, and a diode laser at 785 nm, so to allow for a multi-wavelength excitation. The laser beams at  $\lambda_{\text{exc}} = 633, 561, \text{ and } 785 \text{ nm}$  were focused by means of a microscope objective 50 $\times$  Long Working Distance (Olympus LM-Plan-Fl, NA = 0.5, power of 0.5 mW on samples) mounted on an Olympus BX41 microscope. The used UV line was focused by means of a 60 $\times$  fluorite objective microscope (Olympus UPlan FLN, NA = 0.9, power of 0.5 mW on samples). During the measurements, the scattered radiation was dispersed by a 600 l/mm grating and collected by a silicon CCD as a detector (Synapse, Horiba-Jobin Yvon). For each sample, we chose the excitation wavelength which gave the best Raman response, in order to overcome problems arising from fluorescence contribution to the spectrum. The obtained spectra were compared with those of various databases and literature [16–18].

5) Electron microprobe analysis (EMPA), which was carried out by a JEOL—JXA8230 equipment coupled with a spectrometer EDS—JEOL EX-94310FaL1Q, Silicon drift type. Elemental maps were acquired with the following parameters: HV: 15 keV; probe current: 10 nA; working distance: 11 mm; take off: 40; live time: 50 s.

Criteria for using both portable and not-portable instruments were pursued in order to compare data deriving from both the methodological approaches, in view of future studies that will be performed in situ on unmovable archaeological objects.

### 3. Results and Discussion

#### 3.1. Polarising Optical Microscopy and X-ray Diffraction Analysis

Polarising optical microscopy on thin sections allowed us to investigate the petrographic and textural features of the examined archaeological potsherds. In particular, petrographic analysis focused on the composition of fabrics characterising the types, amounts, size ranges, roundness, and sorting of non-plastic inclusions and types of accessory minerals. The microstructure of the clay matrices was also examined, such as the shape, orientation and size of the voids, and the distribution of inclusions within the fabric. During observations, parameters were determined in accordance with the guidelines proposed by Whitbread [19].

All the investigated samples turned out to be fine pottery with quite homogeneous groundmass and predominant quartz inclusions. The microstructure is characterised by vugs and vesicles, these latter showing slightly preferential orientations with regular shape and smooth surface. Their size varies into the micro-, meso-, and macropores range, with diameters up to 2 mm. The groundmass is characterised by a high optical activity, and its colour in Plane Polarised Light (PPL) varies from being reddish to brown and rarely dark-brown. The inclusions are mainly fine and very fine-grained, and characterised by dominant quartz, sub-angular, rounded, and sub-rounded in shape, along with feldspar and iron oxide(s). Only in samples VQC3 and VQC4, tiny plagioclase crystals were detected. Dark-brown amorphous phases are also present. Some representative photomicrographs are shown in Figure 3, and Table 2 reports the main mineralo-petrographic and textural features for each sample.

XRD analysis confirmed the previous results. In addition, further mineralogical phases such as calcite, diopside, gehlenite, and clay minerals were observed in all samples, whereas gypsum was detected only in VQC1, VQC2, and VQC5 fragments. More details are reported in Table 2.

The mineralogical phase contents obtained from the XRD data analysis can be used to estimate the firing temperature used for the production of the investigated pottery [1,20–24]. More specifically, gehlenite forms from the decomposition products of illite and calcite at 800–850 °C [25,26], whereas diopside is obtained from illite, calcite, and quartz at 850–900 °C [1,21,27]. Therefore, the presence of these phases in the investigated samples indicates a firing temperature of about 850–900 °C. Furthermore, presence of gehlenite can also indicate inhomogeneous and coarser-grained calcite in the source material [27].

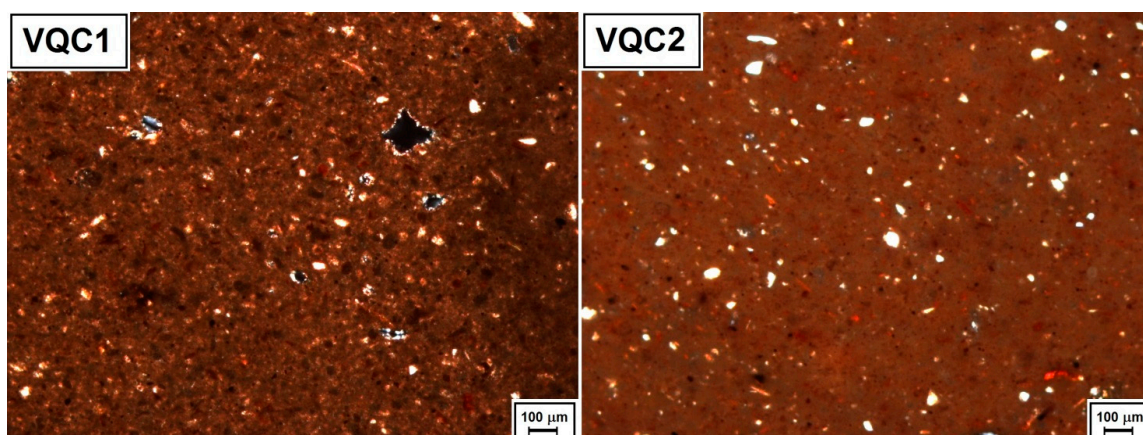


Figure 3. Representative photomicrographs at crossed polars of samples VQC1 and VQC2.

**Table 2.** Main minero-petrographic features of investigated samples as obtained by polarising optical microscopy (POM) and XRD. Notes: Cal = calcite; Di = diopside; Fds = feldspars; Fe-ox = iron oxides; Gh = gehlenite; Gy = gypsum; Pl = plagioclase; Qtz = quartz; Ho = homogeneous; WS = well-sorted; S = sorted; P = present; / = absent; c/f/v = the ratio of coarse, fine, and void components of the fabric (%).

| Minero-Petrographic Features by POM |            |                     |  |         |  |                 |
|-------------------------------------|------------|---------------------|--|---------|--|-----------------|
| Sample                              | Groundmass | Other Inclusions    | Size of Inclusions min-max ( $\mu\text{m}$ ) | Sorting | Common Grain Shape                                     | c/f/v Ratio (%) |
| VQC1                                | Ho         | Qtz, Fds, Fe-ox     | 30–90  | WS      | medium-low sphericity, sub-angular rounding            | 45/40/15        |
| VQC2                                | Ho         | Qtz, Fds, Fe-ox     | 30–300                                       | S to WS | medium-low sphericity, from sub-angular to rounded     | 50/40/10        |
| VQC3                                | Ho         | Qtz, Fds, Fe-ox, Pl | 30–120                                       | WS      | medium-high sphericity, from sub-angular to rounded    | 45/40/15        |
| VQC4                                | Ho         | Qtz, Fds, Fe-ox, Pl | 30–200                                       | WS      | medium-high sphericity, from sub-angular to rounded    | 45/40/15        |
| VQC5                                | Ho         | Qtz, Fds, Fe-ox     | 30–200                                       | S to WS | medium-low sphericity, from sub-angular to sub-rounded | 50/40/10        |

| Mineralogical Phases by XRD |     |     |     |    |    |    |    |                     |
|-----------------------------|-----|-----|-----|----|----|----|----|---------------------|
| Sample                      | Qtz | Fds | Cal | Gh | Di | Pl | Gy | Clay Minerals Group |
| VQC1                        | P   | P   | P   | P  | P  | /  | P  | P                   |
| VQC2                        | P   | P   | P   | P  | P  | /  | P  | P                   |
| VQC3                        | P   | P   | P   | P  | P  | P  | /  | P                   |
| VQC4                        | P   | P   | P   | P  | P  | P  | /  | P                   |
| VQC5                        | P   | P   | P   | P  | P  | /  | P  | P                   |

Regarding calcite, it is probably related to secondary crystallisation processes or to calcium carbonate residue deriving from raw materials [22]. Gypsum could be also interpreted to be of secondary formation, arising from evaporation processes of the groundwater rich in carbonate salts and sulfate, under the surface where fragments were excavated. As well-known, in fact, the long permanence of ceramic finds in burial conditions can alter the original clay matrix composition, as a result of an interaction with the compounds present in the soil [28,29].

Finally, the absence of volcanic inclusions represents a significant factor that allowed us to gain crucial information for the provenance discrimination. Based on these, we can hypothesise that the origin of analysed shards is not local.

### 3.2. X-Ray Fluorescence (XRF) and Micro-Raman Spectroscopy

XRF and micro-Raman analyses were performed on all the five shards, selecting pigmented areas suitable and representative for detections. Measurements were also carried out on the white background and on the ceramic body, the latter just by means of XRF.

The XRF technique was applied, in a non-destructive way, in order to identify the elemental constituents of glazes and pigments of the decorated surfaces of our samples [30–32]. On the other hand, being an element-specific technique, insensitive to the chemical state and/or the molecular environment in which the elements are present, XRF is often not specific enough to guarantee a certain identification. In order to achieve the unambiguous identification of both glazes and pigments, the elemental characterisation needs to be completed by the complementary description of their molecular nature, as achieved by Raman technique, according to a combined approach already successfully applied to a variety of findings, including potteries [33], frescoes [34], and paintings [35].

It is worth remarking that, being that the penetration depth of X-ray source is of the order of a few  $\mu\text{m}$ , which is higher or, at least, similar to the thickness of the investigated coatings, the XRF response will reflect not only the contribution coming from the detected pigments, but also that from the substrate and the preparatory layer (i.e., the ceramic body and the white background). In order to overcome this problem, measurements were also carried out on the ceramic body and the white

background, the latter being present in all the investigated samples. By comparing the data respectively collected on the decorated areas, on the white background, and on the ceramic body, it has been possible to unequivocally distinguish the contribution due to the colouring agents.

The elemental composition, as obtained by the XRF spectral analysis, is summarised in Table 3.

**Table 3.** Elements detected by X-Ray fluorescence (XRF) analysis. For each sample, the key element for pigment identification is marked in bold. The minor or trace elements are presented between brackets.

| Sample | Analysed Area    | Detected Chemical Elements by XRF  |
|--------|------------------|--|
| VQC1   | Light Blue       | S, Pb, K, As, Ca, Cl, Sn (Fe, Ti, <b>Co</b> , Zn, Cd, Mn, Ba, Sr)          |
|        | Orange           | S, Pb, K, Ca, As, Cl, Sn ( <b>Fe</b> , Co, Ti, Ni, Cd, Zn, Mn, Ba)         |
|        | White background | S, Pb, K, Sn, Cl, Ca (As, Fe, Ti, Cd, Mn, Ba)                              |
|        | Ceramic body     | Ca, Fe, K (Ti, Sr, Pb, Mn, Ba, Cr, Zn)                                     |
| VQC2   | Green            | S, Pb, Ca, K, Cl, <b>Cu</b> , Sn (Fe, As, Ti, Sr, Mn, Ba)                  |
|        | Orange           | S, Pb, K, Ca, Cl, Sn, <b>Fe</b> , Sb (As, Cd, Mn)                          |
|        | White background | S, Pb, Ca, K, Fe, Cl (Sn, As, Ti, Sr, Mn, Ba, Cu, Cd, Cr)                  |
|        | Ceramic body     | Ca, Fe, K (Ti, Sr, Pb, Mn, Ba, Cr, Zn)                                     |
| VQC3   | Light Blue       | S, Pb, K, Ca, Sn, As, Cl ( <b>Co</b> , Fe, Ni, Cu, Ti, Zn, Mn, Cd, Ba, Sr) |
|        | Blue             | Pb, S, K, Ca, As, Fe, <b>Co</b> , Sn, Cl (Ni, Ti, Cu, Zn, Mn, Sr, Cd, Ba)  |
|        | Yellow           | Pb, S, K, Ca, Sn, Cl, Fe (As, <b>Sb</b> , Co, Ti, Zn, Cu, Ni, Sr, Mn, Ba)  |
|        | White background | S, Pb, Ca, K, Cl, Fe, As (Sn, Ti, Mn, Sr, Cu, Ba, Zn)                      |
|        | Ceramic body     | Ca, Fe, K (Ti, Sr, Pb, Mn, Ba, Cr, Zn)                                     |
| VQC4   | Green            | S, Pb, k, Cl, Ca, Sn, As ( <b>Cu</b> , Fe, Ti, Zn, Cd, Mn, Ba)             |
|        | Blue             | S, Pb, K, Cl, As, Sn, Ca ( <b>Co</b> , Fe, Ni, Cu, Ti, Zn, Cd, Ba, Mn)     |
|        | White background | S, Pb, K, Ca, Cl, As (Fe, Sn, Ti, Cu, Sr, Mn, Zn, Ba)                      |
|        | Ceramic body     | Ca, Fe, K (Ti, Sr, Pb, Mn, Ba, Cr, Zn)                                     |
| VQC5   | Dark-brown       | S, Pb, K, <b>Mn</b> , Ca, Cl, Sn, As (Fe, Cu, Ba, Cd, Sr)                  |
|        | Light Blue       | S, Pb, K, Cl, Ca, Sn, As, Mn (Fe, <b>Co</b> , Ni, Cu, Cd, Ba)              |
|        | White background | S, Pb, K, Ca, Cl, Sn, As (Fe, Ti, Cd, Mn, Zn, Ba, Sr)                      |
|        | Ceramic body     | Ca, Fe, K (Ti, Sr, Pb, Mn, Ba, Cr, Zn)                                     |

Furthermore, in Figure 4, some representative XRF spectra, respectively collected on the ceramic body of VQC1 (a), on the blue area of VQC3 (b), and on the dark-brown area of VQC5 (c) shards, are reported as examples.

The XRF analysis revealed the presence of lead (Pb) as main constituent in all the investigated areas, pointing to a PbO-based glaze in all fragments, where lead represents a flux [1]. The presence of tin (Sn) is also remarkable, and can be justified by taking into account that, as well known, glazes were opacified by the addition of tin oxide (SnO<sub>2</sub>) [36,37]. Furthermore, these two elements are detected in lower amounts in the ceramic body with respect to the other analysed spots. This allowed us to hypothesise that Pb and Sn are the elements characterising the coating and, comparing our XRF data with literature [1,36,37], we can assume that the analysed fragments are covered by vitreous coatings, typical of glazed majolica pottery.

Cobalt (Co) is the chromophore responsible for blue areas for the VQC3 and VQC4 samples, and light blue shades areas of the VQC1, VQC3, and VQC5 fragments. The blue shades of glaze can be obtained by dissolution of Co<sup>2+</sup> ions in the glassy phase during firing. When the Co<sup>2+</sup> ion concentration is higher than a few weight percent, Co-silicate or Co-aluminate compounds precipitate and they can be revealed in the glaze [38]. In addition, the elemental association of Co-Fe-Ni-As was observed

in all of the investigated shards where blue shades were present. According to literature [1,2,38–42], this occurrence is consistent with the use of cobalt obtained from the Erzgebirge mining region in Saxony (Germany), an important pigment production centre with exports to all parts of Europe. Low amounts of Ni associated to Co are also characteristic of blue pigments used in majolica potteries from Italy [43] and in Valencian ceramics [44]. These Co–Ni-based pigments can be produced by roasting of zaffre (Co–Ni–As minerals) at high temperatures, providing some insight into the production method of the Co-based blue pigment.

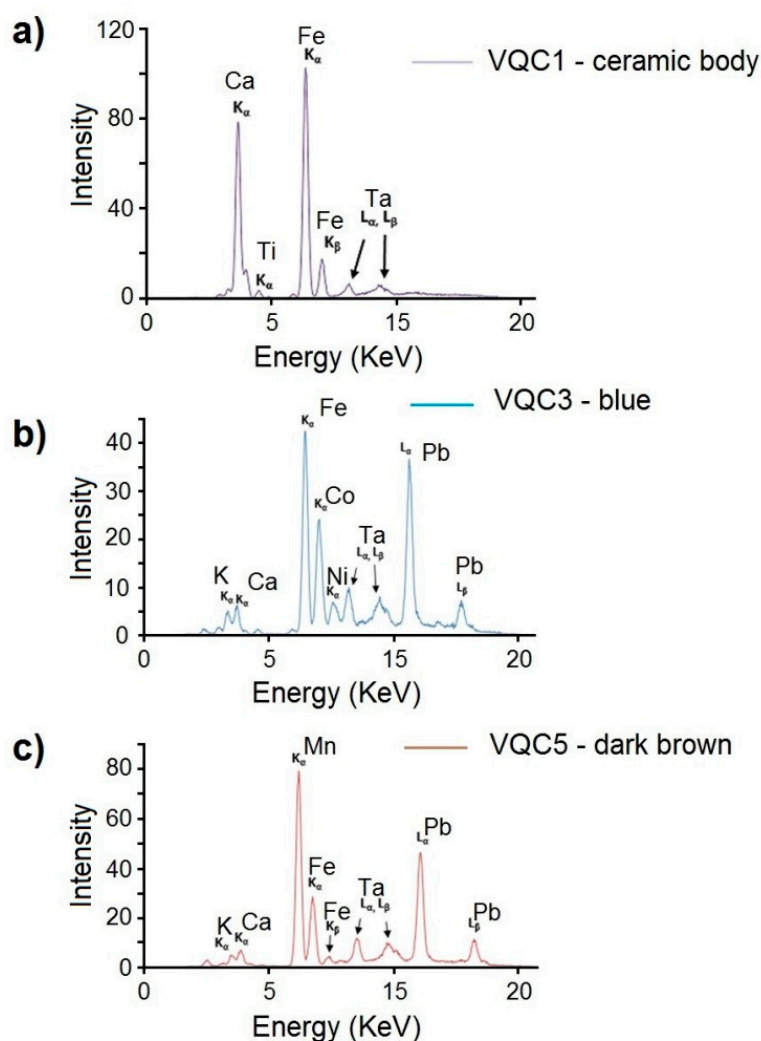


**Figure 4.** Representative XRF spectra collected on the (a) ceramic body of the VQC1 sample, (b) blue area of the VQC3 sample, and (c) dark-brown area of the VQC5 sample.

Looking at the elemental composition collected at the yellow area of the glazed surface of sample VQC3, the detection of elements such as Pb, Sn, and Sb indicate the use of lead (II) antimonate or lead tin yellow pigments [45]. However, since Sn is also present in the glaze as an opacifier (SnO<sub>2</sub>), XRF analysis alone cannot unambiguously identify the yellow pigment used [46]. The presence of Mn and Fe at dark-brown decorations, only present in sample VQC5, suggests the use of earth pigments, most likely umber (iron oxide with about 6–15% of MnO<sub>2</sub> + clay + silica) [47]. In addition, XRF analyses identified the use of copper (Cu) at green decorations in samples VQC2 and VQC4, and iron (Fe) as the chromophore element responsible for the orange areas of VQC1 and VQC2 shards.

Finally, as far as the ceramic body is concerned, calcium (Ca) and iron (Fe) were the main chemical elements detected, certainly due to the mineralogical phases constituting the ceramic paste.



Raman spectra were collected on different spots of the coloured areas of some of the fragments under analysis. In particular, measurements were performed on the light blue and white areas of the VQC1 sample, on the orange area of VQC2, and on the dark-brown area of VQC5. The obtained results are reported in Figure 5.

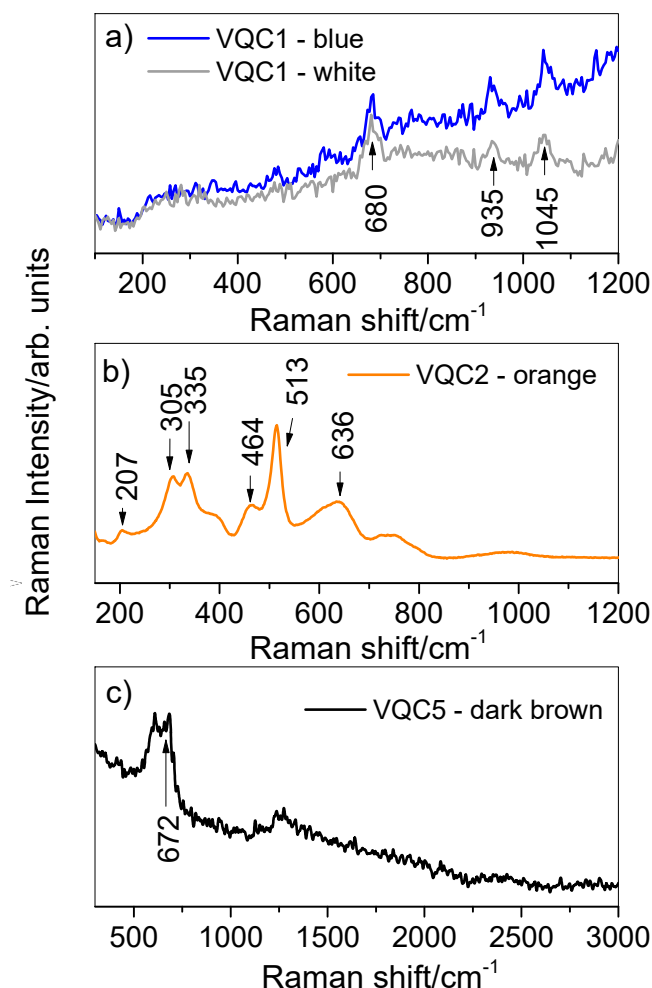


**Figure 5.** Representative Raman spectra recorded on (a) blue and white colouring areas of the VQC1 sample (excitation wavelength of 364 nm), (b) orange area of the VQC2 sample (excitation wavelength of 561 nm), and (c) dark-brown area of the VQC5 sample (excitation wavelength of 785 nm). It is worth remarking that, in the case of VQC2 sample, the good quality of the spectrum is justified by Raman scattering in resonance conditions.

In addition, analyses have been also performed on the white background of sample VQC1 (spectrum not reported).

The Raman profiles of both blue and white areas of the VQC1 fragment showed the characteristic peaks of calcium antimonate ( $\text{CaSb}_2\text{O}_7$ ) at about 680, 935, and 1045  $\text{cm}^{-1}$ . Ca-antimonates, which are white in colour, are the most common opacifiers widely used since Roman glassmaking and for a very long time, i.e., from around 1500 B.C. until modern times [48–51]. In particular, as far as the light blue sampled area is concerned, the presence of Ca-antimonate is usually associated to ionic chromophores, such as cobalt ( $\text{Co}^{2+}$ ) responsible for the blue colour [52]. In our case, this is supported by the XRF analysis which showed the presence of cobalt (Co) in such a sample (VQC1) (Table 3).

The Raman profile collected on the orange area of the VQC2 shard revealed the presence of another opacifier agent, Pb-antimonate ( $\text{Pb}_2\text{Sb}_2\text{O}_7$ ), with characteristic peaks at about 305, 335, 464,

and  $513\text{ cm}^{-1}$ . In addition, the peaks at about  $207$  and  $636\text{ cm}^{-1}$  can be ascribed to cuprite ( $\text{Cu}_2\text{O}$ ), probably responsible for the red/orange colour.

Regarding the dark-brown area of the VQC5 fragment, a single broad band centred at about  $672\text{ cm}^{-1}$  was detected, which could be associated to the presence of magnetite ( $\text{Fe}_3\text{O}_4$ ), an iron oxide commonly mixed to clay to obtain ochre pigments [53,54] or natural earths, the latter known as umber and characterised by the presence of manganese dioxide [55]. For this sample, X-ray fluorescence analysis evidenced the presence of both Mn and Fe, so the use of umber can be hypothesised. UMBER pigment, containing hydrated iron and manganese oxides, appeared for the first time in the late 15th century. It is also known as raw umber, and when heated it becomes of a more intense brown colour, known as burnt umber [56].

As far as the green areas of all the investigated samples are concerned, the Raman technique did not give reliable results, which is in agreement with the use of  $\text{Cu}^{2+}$  ions dispersed in the glassy matrix for green decorations [1,42].

### 3.3. EMPA-EDS

EMPA-EDS analysis was carried out working on individual colour fragments chipped-off from the sides of the shards, resulting as the decisive investigation and giving further confirmation to the previous ones.

Concerning morphology, the presence of a dual layer of ceramic body/decorative glazed coatings, was put into evidence (Figure 6).

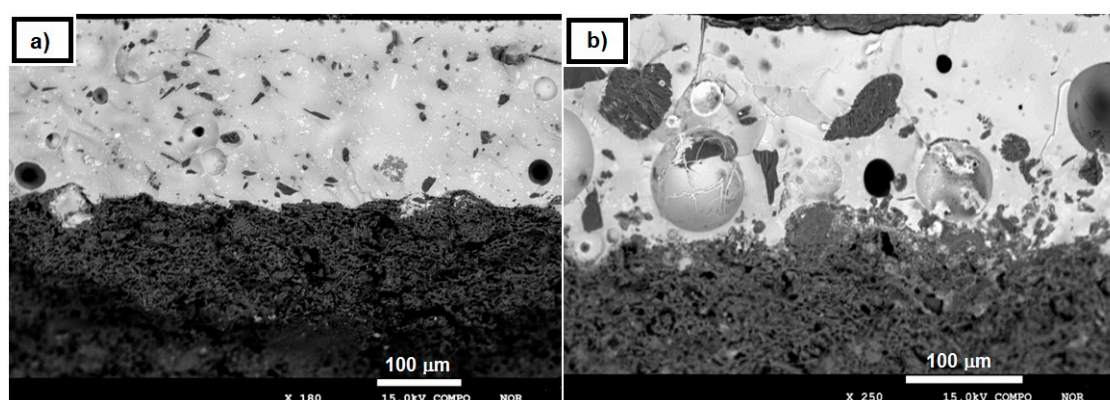


**Figure 6.** Representative electron microprobe analysis coupled with energy dispersive spectrometry (EMPA-EDS) images showing some morphological features of the VQC2 (a) and VQC3 (b) samples with evidence of a dual layer, ceramic body/superficial coating.

No further layer was distinguished within the coating. The microstructures of the glazes as seen by EMPA-EDS show thicknesses less than  $200\text{ }\mu\text{m}$  and a distribution of bright lead–tin–oxide particles, air bubbles, and quartz grains casually scattered in the glaze thickness [57]. In particular, air bubbles, having diameters of up to  $50\text{ }\mu\text{m}$ , are probably due to the formation of gaseous products during heating [58,59].

Regarding the chemical analysis, five measurements were performed for each investigated sample, and the average value was considered as representative of the chemical elemental composition. Table 4 reports the EMPA-EDS chemical data (wt%) of all the investigated samples, with the main key elements responsible for coloured areas marked in bold.

**Table 4.** EMPA-EDS chemical data (wt%) of the examined samples and related standard deviation. The main key elements responsible for coloured areas are marked in bold.

|                  |                  | Detected Chemical Elements by EMPA-EDS |                   |      |                                |                  |                               |                  |              |                                |                  |              |             |                                |             |             |
|------------------|------------------|--|-------------------|------|--------------------------------|------------------|-------------------------------|------------------|--------------|--------------------------------|------------------|--------------|-------------|--------------------------------|-------------|-------------|
| Sample           | Analysed Area    | CaO                                    | Na <sub>2</sub> O | MgO  | Al <sub>2</sub> O <sub>3</sub> | SiO <sub>2</sub> | P <sub>2</sub> O <sub>5</sub> | K <sub>2</sub> O | FeO          | As <sub>2</sub> O <sub>3</sub> | SnO <sub>2</sub> | PbO          | CoO         | Cr <sub>2</sub> O <sub>3</sub> | CuO         | MnO         |
| VQC1             | Blue             | 1.35                                   | 1.25              | 0.31 | 4.56                           | 51.78            |                               | 6.69             | 0.82         | 0.09                           | 1.26             | 31.73        | <b>0.16</b> |                                |             |             |
|                  | σ                | 0.09                                   | 0.10              | 0.04 | 0.03                           | 5.12             |                               | 0.40             | 0.05         | 0.03                           | 0.13             | 0.83         | <b>0.03</b> |                                |             |             |
|                  | Light Blue       | 1.45                                   | 1.14              | 0.26 | 4.15                           | 52.15            | 0.35                          | 5.62             | 0.45         | 0.10                           | 1.20             | 33.07        | <b>0.06</b> |                                |             |             |
|                  | σ                | 0.20                                   | 0.15              | 0.03 | 0.05                           | 4.88             | 0.05                          | 0.72             | 0.03         | 0.02                           | 0.15             | 1.23         | <b>0.03</b> |                                |             |             |
|                  | Orange           | 1.87                                   | 1.31              | 0.34 | 3.28                           | 40.97            | 2.93                          | 6.83             | <b>10.10</b> | 0.24                           |                  |              |             |                                |             |             |
|                  | σ                | 0.25                                   | 0.88              | 0.05 | 0.10                           | 3.35             | 0.50                          | 0.88             | <b>1.22</b>  | 0.02                           |                  |              | 1.48        |                                |             |             |
|                  | White background | 1.31                                   | 1.03              | 0.20 | 3.53                           | 48.08            |                               | 5.80             | 0.29         | 0.04                           | 1.82             | 37.90        |             |                                |             |             |
| σ                | 0.08             | 0.12                                   | 0.07              | 0.17 | 2.45                           |                  | 0.30                          | 0.04             | 0.01         | 0.40                           | 0.97             |              |             |                                |             |             |
| VQC2             | Blue             | 1.00                                   | 0.99              | 0.12 | 2.39                           | 47.06            |                               | 4.20             | 0.81         | 0.15                           | 0.86             | 42.21        | <b>0.21</b> |                                |             |             |
|                  | σ                | 0.05                                   | 0.10              | 0.04 | 0.30                           | 4.48             |                               | 0.60             | 0.05         | 0.03                           | 0.12             | 1.34         | <b>0.05</b> |                                |             |             |
|                  | Green            | 1.01                                   | 1.08              | 0.18 | 3.26                           | 44.40            |                               | 4.19             |              | 0.15                           | 2.02             | 40.00        |             |                                | <b>3.70</b> |             |
|                  | σ                | 0.05                                   | 0.07              | 0.05 | 0.61                           | 3.07             |                               | 0.18             |              | 0.02                           | 0.55             | 0.89         |             |                                | 0.80        |             |
|                  | Orange           | 0.61                                   | 1.39              | 0.25 | 2.77                           | 44.04            |                               | 5.92             | <b>6.95</b>  | 0.14                           |                  | 37.89        |             | 0.04                           |             |             |
|                  | σ                | 0.10                                   | 0.56              | 0.05 | 0.30                           | 3.48             |                               | 0.67             | <b>0.07</b>  | 0.02                           |                  | 1.78         |             | 0.01                           |             |             |
|                  | White background | 0.79                                   | 1.20              | 0.13 | 3.36                           | 49.45            |                               | 4.27             | 0.13         | 0.10                           | 1.18             | 39.39        |             |                                |             |             |
| σ                | 0.06             | 0.10                                   | 0.06              | 0.22 | 3.15                           |                  | 0.80                          | 0.03             | 0.01         | 0.40                           | 1.12             |              |             |                                |             |             |
| VQC3             | Blue             | 1.43                                   | 1.53              | 0.24 | 3.73                           | 56.24            |                               | 4.13             | 1.40         |                                |                  | 30.49        | <b>0.81</b> |                                |             |             |
|                  | σ                | 0.12                                   | 0.10              | 0.04 | 0.89                           | 6.02             |                               | 0.70             | 0.10         |                                |                  | 1.15         | <b>0.11</b> |                                |             |             |
|                  | Light Blue       | 1.88                                   | 1.53              |      | 4.16                           | 61.86            |                               | 4.51             | 0.59         | 0.11                           | 1.04             | <b>24.21</b> | 0.11        |                                |             |             |
|                  | σ                | 0.15                                   | 0.21              |      | 0.14                           | 4.94             |                               | 0.63             | 0.03         | 0.02                           | 0.15             | <b>0.98</b>  | 0.02        |                                |             |             |
|                  | Yellow           | 1.15                                   | 1.97              | 0.30 | 5.34                           | 68.54            |                               | <b>5.65</b>      | 0.33         |                                | 1.52             | <b>15.20</b> |             |                                |             |             |
|                  | σ                | 0.01                                   | 0.16              | 0.07 | 0.93                           | 5.58             |                               | <b>0.86</b>      | 0.05         |                                | 0.25             | <b>1.68</b>  |             |                                |             |             |
|                  | Green            | 0.82                                   | 2.34              | 0.25 | 4.15                           | 65.36            |                               | 5.93             | 1.50         | 0.13                           | 1.20             | 17.84        | 0.48        |                                |             |             |
| σ                | 0.04             | 0.10                                   | 0.05              | 0.72 | 3.67                           |                  | 0.23                          |                  | 0.02         | 0.05                           | 0.98             | <b>0.03</b>  |             |                                |             |             |
| White background | 3.02             | 2.07                                   | 0.44              | 3.97 | 64.94                          |                  | 5.80                          | 0.49             |              | 1.69                           | 17.58            |              |             |                                |             |             |
| σ                | 0.10             | 0.22                                   | 0.07              | 0.32 | 4.55                           |                  | 0.45                          | 0.05             |              | 0.56                           | 1.11             |              |             |                                |             |             |
| VQC4             | Blue             | 2.09                                   | 1.95              | 0.45 | 3.51                           | 51.55            |                               | <b>3.92</b>      | 0.68         |                                | 1.20             | <b>34.50</b> | 0.15        |                                |             |             |
|                  | σ                | 0.09                                   | 0.11              | 0.04 | 0.77                           | 5.86             |                               | 0.88             | 0.12         |                                | 0.05             | 2.22         | 0.04        |                                |             |             |
|                  | Green            | 2.53                                   | 1.98              | 0.55 | 3.56                           | 51.26            |                               | <b>3.70</b>      | 0.64         |                                | 0.78             | <b>33.92</b> |             |                                | 1.08        |             |
|                  | σ                | 0.10                                   | 0.29              | 0.04 | 0.79                           | 4.48             |                               | 0.24             | 0.03         |                                | 0.08             | 1.54         |             |                                | 0.12        |             |
|                  | White background | 1.98                                   | 2.27              | 0.53 | 4.29                           | 54.45            |                               | 4.13             | 0.69         |                                | <b>0.79</b>      | 30.87        |             |                                |             |             |
| σ                | 0.06             | 0.09                                   | 0.06              | 0.62 | 3.97                           |                  | 0.44                          | 0.04             |              | <b>0.08</b>                    | 1.44             |              |             |                                |             |             |
| VQC5             | Light Blue       | 1.45                                   | 1.00              | 0.24 | 2.98                           | 45.56            |                               | 4.06             | 0.57         |                                | <b>0.87</b>      | 43.08        | 0.19        |                                |             |             |
|                  | σ                | 0.15                                   | 0.15              | 0.03 | 0.05                           | 4.54             |                               | 0.89             | 0.03         |                                | <b>0.15</b>      | 2.18         | 0.03        |                                |             |             |
|                  | Dark-brown       | 1.56                                   | 1.23              | 0.41 | 3.15                           | 45.23            |                               | 4.00             | 0.65         |                                | 0.72             | 42.32        |             |                                |             | <b>0.73</b> |
|                  | σ                | 0.15                                   | 0.22              | 0.02 | 0.20                           | 5.78             |                               | 0.76             | 0.05         |                                | 0.05             | 2.78         |             |                                |             | <b>0.05</b> |
|                  | White background | 2.49                                   | 0.86              | 0.34 | 2.92                           | 40.30            |                               | 3.40             | 0.69         |                                | 3.26             | 45.74        |             |                                |             |             |
| σ                | 0.25             | 0.12                                   | 0.06              | 0.44 | 3.78                           |                  | 0.32                          | 0.04             |              | 0.33                           | 2.78             |              |             |                                |             |             |

Results revealed the presence of a glassy coating with a high concentration of silica ( $\text{SiO}_2$ ), which is the main component of this type of coating. Furthermore, all the other oxides generally used for vitreous materials, i.e., calcium ( $\text{CaO}$ ), sodium ( $\text{Na}_2\text{O}$ ), magnesium ( $\text{MgO}$ ), aluminium ( $\text{Al}_2\text{O}_3$ ), and potassium and lead ( $\text{PbO}$ ) oxides, were detected. This last one, in particular, is known for giving considerable brightness to the glazes. Cassiterite ( $\text{SnO}_2$ ) was also detected, which is the opaque agent most used in the past, especially during the Renaissance.  $\text{SnO}_2$  gives a whitish surface, providing a compact base suitable for the application of chromatic decorations. Finally, arsenic oxide ( $\text{As}_2\text{O}_3$ ) was also detected in some fragments, whose use as opacifier agent is already reported in literature [60].

Taking into account the absence of additional layers within the coating (Figure 6), analyses prove that the chromophore elements are dispersed in the glazing. Spreading, typical of glazes, at high temperatures causes a dissolution action on the colouring agents, causing colour diffusion in the glass layer, especially when the coating composition is chemically aggressive [42].

Regarding the characterisation and identification of pigments, some doubts remained for the areas with yellow and orange motifs. On the contrary, for the blue, dark-brown, and green pigments, all previously reported data are confirmed. In detail, in the case of the yellow area of the VQC3 sample, the EMPA-EDS spot analysis confirmed one of the two hypotheses previously presumed by the XRF dataset: The identification of tin and lead oxides in the yellow area prove that a lead–tin yellow, and not a lead (II) antimonite, was used as pigment for such painted shards [46]. For the orange areas of the VQC1 and VQC2 samples, iron oxide(s) (typical of ochre pigments) remains the dominant chromophore. Probably, the detection of peaks ascribable to cuprite ( $\text{Cu}_2\text{O}$ ) and detected by means of Raman technique, was due to the addition of such a mineral to make the colour more intense.

#### 4. Conclusions

The achieved results suggest that none of the above analytical investigations can provide, alone, unequivocal interpretation about the characterisation of the examined painted pottery shards dated back to the 16th century, coming from the archaeological context of Villa dei Quintili (Rome, Italy). A multi-technique approach was then applied, and the intersection of the whole dataset, together with the comparison with literature, became mandatory, in view of some deeper considerations on the samples under study, allowing in particular their recognition as majolica of the Renaissance period. Investigated shards exhibit both open and closed shapes, and show distinctive decorative motifs and colours. Minero-petrographic features, observed by means of polarising optical microscopy (POM) on thin and stratigraphic sections of the ceramic bodies, and by X-ray diffraction (XRD), revealed significant similarities between samples, probably indicating a similar production technology, especially regarding the firing temperature and raw materials used. Furthermore, considering the absence of volcanic fragments, a non-local origin of the investigated ceramic shards was hypothesised. In this regard, further study will be performed.

In addition, a multi-analytical approach involving micro-Raman spectroscopy, X-Ray fluorescence (XRF), and electron microprobe analysis coupled with energy dispersive spectrometry (EMPA-EDS) allowed the characterisation of the composition of pigments in decorative glazed coatings of the fragments. From the results, the yellow pigment was identified as “lead–tin yellow”, the dark-brown pigment as “umber” deriving from the use of earth pigments, the green pigment as a “Cu-green” pigment, and the blue pigment as a “cobalt blue”. Finally, the orange pigment was identified as an ochre with the probable presence of cuprite.

In this context, the characterisation of archaeological painted pottery and the identification of pigments through an archaeometric and multi-analytical approach was needful in order to confirm their importance in the context of the Villa, also highlighting that the discovery of such fragments can be attributed to the use of the Villa as a quarry for the extraction of materials with respect to its past use as a residential area [4,8,61].

**Author Contributions:** Conceptualization, G.G.; data curation, M.R., N.R., V.C., and B.F.; formal analysis, M.R., G.P., and V.V.; funding acquisition, M.F.L.R.; investigation, M.R., S.A.R., and L.R.; methodology, D.M.; supervision, V.C., V.V., and M.F.L.R.; validation, D.M.; writing—original draft, M.R.; writing—review & editing, M.F.L.R.

**Funding:** This research received no external funding.

**Acknowledgments:** The anonymous reviewers are thanked for critically reading the manuscript and suggesting substantial improvements.

**Conflicts of Interest:** The authors declare no conflict of interest.

## References

- Gajić-Kvašček, M.; Bikić, V.; Wright, V.J.; Evans, I.R.; Damjanović-Vasilić, L. Archaeometric study of 17th/18th century painted pottery from the Belgrade Fortress. *J. Cult. Herit.* **2018**, *32*, 9–21. [[CrossRef](#)]
- Ferreira, L.F.V.; Machado, I.F.; Casimiro, T.M.; Pereira, M.F.C.; Santos, L.F. Portuguese blue-on-blue 16th–17th century pottery. *Archaeometry* **2018**, *60*, 695–712. [[CrossRef](#)]
- Ricci, A. La villa dei Quintili sulla via Appia Antica: Riuso e spoliazione. *Seminari di Archeologia Cristiana* **1991**, *67*, 467–469.
- D’Agostino, S.; Bellomo, M. Excavation, restoration and conservation of archaeological sites. The Villa dei Quintili on the Appia Antica in Rome. *WIT Trans. Built Environ.* **1999**, *6*, 451–460.
- Frontoni, R. *Forma Urbis-Itinerari Nascosti di Roma Antica*; ANNO: Rome, Italy, 2000.
- Paris, R. Appia Antica. In *Villa dei Quintili*; Tomei, M.A., Ed.; Memorie dal Sottosuolo: Verona, Italy, 2006.
- Frontoni, R.; Galli, G. Calce e calcara nella Villa dei Quintili. *Arkos Scienza e Restauro* **2010**, *25*, 66–73.
- Belfiore, C.M.; Ricca, M.; la Russa, M.F.; Ruffolo, S.A.; Galli, G.; Barca, D.; Malagodi, M.; Vallefucio, M.; Sprovieri, M.; Pezzino, A. Provenance study of building and statuary marbles from the Roman archaeological site of “Villa dei Quintili” Rome, Italy. *Ital. J. Geosci.* **2016**, *135*, 236–249. [[CrossRef](#)]
- Bruun, C. Fistule acuarie e propriety terrier nel suburbium. In *Suburbium: Il Suburbio di Roma dalla Crisi del Sistema delle Ville a Gregorio Magno*; Pergola, P., Valenziani, R.S., Volpe, R., Eds.; École Française de Rome: Rome, Italy, 2003; pp. 485–501.
- Paris, R. *Via Appia. La Villa dei Quintili. Collana Soprintendenza Archeologica di Roma*; Mondadori Electa: Milano, Italy, 2000.
- Frontoni, R.; Galli, G.; Paris, R.; Rotondi, A. *Forma Urbis—Itinerari Nascosti di Roma Antica, Anno XVII*; ANNO: Roma, Italy, 2012.
- Panagopoulou, A.; Lampakis, D.; Christophilos, D.; Beltsios, K.; Ganetsos, T. Technological examination of Iznik ceramics by SEM-EDX, Raman, XRD, PLM: A case study. *Sci. Cult.* **2018**, *4*, 27–33.
- Rahim, N.S.A. Analytical study and conservation of archaeological Terra Sigillata ware from Roman Period, Tripoli, Libya. *Sci. Cult.* **2016**, *2*, 19–27.
- Findik, N.Ö.; Akyol, A.A.; Sari, N. Archaeometric analyses of Hasankeyf unglazed ceramics. *Mediterr. Archaeol. Archaeom.* **2014**, *14*, 261–271.
- García-Iñáñez, J.; Garrigós, J.B.I.; Fernández, M.M.I.; Esparraguera, J.M.G.I.; Cerdà, J.A.C.I. Archaeometric characterization of Middle Age and Renaissance tin lead glazed pottery from Barcelona. In *Archaeometric and Archaeological Approaches to Ceramics*; BAR International Series, 1691; Yona Waksman, S., Ed.; Archaeopress: Oxford, UK, 2007; p. 175.
- Bell, I.M.; Clark, R.J.H.; Gibbs, P.J. Raman spectroscopic library of natural and synthetic pigments pre-~ 1850 AD. *Spectrochim. Acta A* **1997**, *53*, 2159–2179. [[CrossRef](#)]
- Buzgar, N.; Apopei, A.I.; Buzatu, A. Database of Raman Spectroscopy. 2009. Available online: [rdrs.uaic.ro](http://rdrs.uaic.ro) (accessed on 16 April 2019).
- Lafuente, B.; Downs, R.T.; Yang, H.; Stone, N. The power of databases: The RRUFF project. In *Highlights in Mineralogical Crystallography*; Armbruster, T., Danisi, R.M., Eds.; W. De Gruyter: Berlin, Germany, 2015; pp. 1–30.
- Whitbread, I.K. *Greek Transport Amphorae. A Petrological and Archaeological Study*; The British School at Athens: Athens, Greece, 1995.
- Aloise, P.; Ricca, M.; la Russa, M.F.; Ruffolo, S.A.; Belfiore, C.M.; Padeletti, G.; Crisci, G.M. Diagnostic analysis of stone materials from underwater excavations: The case study of the Roman archaeological site of Baia Naples, Italy. *Appl. Phys. A* **2014**, *1143*, 655–662. [[CrossRef](#)]

21. Barca, D.; la Russa, M.F.; Crisci, G.M. Technological and geochemical study of two red figured vases of unknown provenance by various analytical techniques. *Appl. Phys. A* **2010**, *1003*, 911–917. [[CrossRef](#)]
22. Montero, M.A.; Jordán, M.M.; Almendro-Candel, M.B.; Sanfeliu, T.; Hernández-Crespo, M.S. The use of a calcium carbonate residue from the stone industry in manufacturing of ceramic tile bodies. *Appl. Clay Sci.* **2009**, *43*, 186–189. [[CrossRef](#)]
23. Ricca, M.; Comite, V.; la Russa, M.F.; Barca, D. Diagnostic analysis of bricks from the underwater archaeological site of Baia Naples, Italy: Preliminary results. *Rend. Online Soc. Geol. Ital.* **2016**, *38*, 85–88. [[CrossRef](#)]
24. Rovella, N.; Comite, V.; Ricca, M. The methodology of investigation on red-and black-figured pottery of unknown provenance. *Int. J. Conserv. Sci.* **2016**, *72*, 954–964.
25. Maritan, L.; Nodari, L.; Mazzoli, C.; Milano, A.; Russo, U. Influence of firing conditions on ceramic products: Experimental study on clay rich in organic matter. *Appl. Clay Sci.* **2006**, *31*, 1–15. [[CrossRef](#)]
26. Riccardi, M.P.; Messiga, B.; Duminuco, P. An approach to the dynamics of clayfiring. *Appl. Clay Sci.* **1999**, *15*, 393–409. [[CrossRef](#)]
27. Kreimeyer, R. Some notes on the Firing Colour of Clay Bricks. *Appl. Clay Sci.* **1987**, *2*, 175–183. [[CrossRef](#)]
28. Garrigós, J.B.I. Alteration and contamination of archaeological ceramics: The perturbation problem. *J. Archaeol. Sci.* **1999**, *26*, 29–313.
29. Messina, M.; Arcifa, L.; Barone, G.; Finocchiaro, C.; Mazzoleni, P. Islamic Pottery Production in Eastern Sicily (10th–11th Centuries): Preliminary archaeometric data on local and imported products from Paternò (Sicily). *Mediterr. Archaeol. Archaeom.* **2018**, *5*, 207–223.
30. Crupi, V.; Majolino, D.; Venuti, V.; Barone, G.; Mazzoleni, P.; Pezzino, A.; la Russa, M.F.; Ruffolo, S.A.; Bardelli, F. Non-destructive identification of green and yellow pigments: The case of some Sicilian Renaissance glazed pottery. *Appl. Phys. A* **2010**, *100*, 845–853. [[CrossRef](#)]
31. Crupi, V.; Galli, G.; la Russa, M.F.; Longo, F.; Maisano, G.; Majolino, D.; Malagodi, M.; Pezzino, A.; Ricca, M.; Rossi, B.; et al. Multi-technique investigation of Roman decorated plasters from Villa dei Quintili Rome, Italy. *Appl. Surf. Sci.* **2015**, *349*, 924–930. [[CrossRef](#)]
32. Crupi, V.; Fazio, B.; Fiocco, G.; Galli, G.; la Russa, M.F.; Licchelli, M.; Majolino, D.; Malagodi, M.; Ricca, M.; Ruffolo, S.A.; et al. Multi-analytical study of Roman frescoes from Villa dei Quintili Rome, Italy. *J. Archaeol. Sci. Rep.* **2018**, *21*, 422–432. [[CrossRef](#)]
33. Scarpelli, R.; Clark, R.J.; de Francesco, A.M. Archaeometric study of black-coated pottery from Pompeii by different analytical techniques. *Spectrochim. Acta A* **2014**, *120*, 60–66. [[CrossRef](#)]
34. Appolonia, L.; Vaudan, D.; Chatel, V.; Aceto, M.; Mirti, P. Combined use of FORS, XRF and Raman spectroscopy in the study of mural paintings in the Aosta Valley (Italy). *Anal. Bioanal. Chem.* **2009**, *395*, 2005–2013. [[CrossRef](#)]
35. Casuccio, G.; Bunker, K.; Kennedy, S.; Sparrow, M.; Pacolay, B.; Ioannidis, P.; Foulke, R. Portable XRF and Raman analysis of a ‘Modigliani’ signature painting. *Microsc. Microanal.* **2012**, *18*, 958–959. [[CrossRef](#)]
36. Tite, M.S.; Pradell, T.; Shortland, A. Discovery, production and use of tin-based opacifiers in glasses, enamels and glazes from the Late Iron Age onwards: A reassessment. *Archaeometry* **2008**, *50*, 67–84. [[CrossRef](#)]
37. Tite, M.S. The production technology of Italian maiolica: A reassessment. *J. Archaeol. Sci.* **2009**, *36*, 2065–2080. [[CrossRef](#)]
38. Colomban, P.; Zhang, Y.; Zhao, B. Non-invasive Raman analyses of Chinese huafalang and related porcelain wares. Searching for evidence for innovative pigment technologies. *Ceram. Int.* **2017**, *43*, 12079–12088. [[CrossRef](#)]
39. Gratuze, B.; Soulier, I.; Barradon, J.N.; Foy, D. De l’origine du cobalt dans les verres. *Rev. Archeom.* **1992**, *16*, 97–108. [[CrossRef](#)]
40. Gratuze, B.; Soulier, I.; Blet, M.; Vallauri, L. De l’origine du cobalt: Du verre à lacéramique. *Rev. Archeom.* **1996**, *20*, 77–94.
41. Zucchiatti, A.; Bouquillon, A.; Katona, I.; D’Alessandro, A. The “Della Robbia blue”: A case study for the use of cobalt pigments in ceramics during the Italian renaissance. *Archaeometry* **2006**, *48*, 131–152. [[CrossRef](#)]
42. Colomban, P.; Arberet, L.; Kirmizi, B. On-site analysis of 17th–18th centuries Limoges enamels. Arsenic and the technological relationship between enamelled Limoges and Chinese wares. *Ceram. Int.* **2017**, *43*, 10158–10165. [[CrossRef](#)]
43. Dell’Aquila, C.; Laviano, R.; Vurro, F.J. Chemical and mineralogical investigations of majolicas 16th–19th centuries from Laterza, southern Italy. *Geol. Soc.* **2006**, *257*, 151–162. [[CrossRef](#)]

44. Roldán, C.; Coll, J.; Ferrero, J. EDXRF analysis of blue pigments used in Valencian ceramics from the 14th century to modern times. *J. Cult. Herit.* **2006**, *7*, 134–138. [[CrossRef](#)]
45. Schurr, M.R.; Donohue, P.H.; Simonetti, A.; Dawson, E.L. Multi-element and lead isotope characterization of early nineteenth century pottery sherds from Native American and Euro-American sites. *J. Archaeol. Sci. Rep.* **2018**, *20*, 39–399. [[CrossRef](#)]
46. Šefců, R.; Chlumská, Š.; Hostašová, A. An investigation of the lead tin yellows type I and II and their use in Bohemian panel paintings from the Gothic period. *Herit. Sci.* **2015**, *3*, 1–15. [[CrossRef](#)]
47. Sandalinas, C.; Ruiz-Moreno, S.; López-Gil, A.; Miralles, J. Experimental confirmation by Raman spectroscopy of a Pb–Sn–Sb triple oxide yellow pigment in sixteenth-century Italian pottery. *J. Raman Spectrosc.* **2006**, *37*, 1146–1153. [[CrossRef](#)]
48. Bevilacqua, N.; Borgioli, L.; Gracia, I.A. *I Pigmenti-nell'arte. Dalla Preistoria Alla Rivoluzione Industrilae*; Matteini: Saonara, Italy, 2010.
49. Shortland, A.J. The use and origin of antimonate colorants in early Egyptian glass. *Archaeometry* **2002**, *44*, 517–530. [[CrossRef](#)]
50. Freestone, I.C.; Stapleton, C.P.; Rigby, V. The production of red glass and enamel in the Late Iron Age, Roman and Byzantine periods. In *Through a Glass Brightly: Studies in Byzantine and Medieval Art and Archaeology*; Entwistle, C., Buckton, D., Eds.; Oxbow Books: Oxford, UK, 2003; ISBN 978-1785702518.
51. Lahlil, S.; Biron, I.; Galois, L.; Morin, G. Technological processes to produce antimonate opacified glass throughout history. *Annales du* **2009**, *17*, 571–578.
52. Molina, G.; Odin, G.P.; Pradell, T.; Shortland, A.J.; Tite, M.S. Production technology and replication of lead antimonate yellow glass from New Kingdom Egypt and the Roman Empire. *J. Archaeol. Sci.* **2014**, *41*, 171–184. [[CrossRef](#)]
53. Maltoni, S.; Silvestri, A. Investigating Production Technologies of Roman Glass Tesserae from Northeastern Italy. *Minerals* **2018**, *86*, 255. [[CrossRef](#)]
54. Legodi, M.; de Waal, D. The preparation of magnetite, goethite, hematite and maghemite of pigment quality from mill scale iron waste. *Dyes Pigments* **2007**, *74*, 161–168. [[CrossRef](#)]
55. Montagner, C.; Sanches, D.; Pedroso, J.; Melo, M.J.; Vilarigues, M. Ochres and earths: Matrix and chromophores characterization of 19th and 20th century artist materials. *Spectrochim. Acta A* **2013**, *103*, 409–416. [[CrossRef](#)]
56. Hradil, D.; Grygar, T.; Hradilová, J.; Bezdička, P. Clay and iron oxide pigments in the history of painting. *Appl. Clay Sci.* **2003**, *22*, 223–236. [[CrossRef](#)]
57. Genestar, C.; Pons, C. Earth pigments in painting: Characterisation and differentiation by means of FTIR spectroscopy and SEM-EDS microanalysis. *Anal. Bioanal. Chem.* **2005**, *3822*, 269–274. [[CrossRef](#)]
58. Matin, M.; Tite, M.; Watson, O. On the origins of tin-opacified ceramic glazes: New evidence from early Islamic Egypt, the Levant, Mesopotamia, Iran, and Central Asia. *J. Archaeol. Sci.* **2018**, *97*, 42–66. [[CrossRef](#)]
59. Campanella, L.; Casoli, A.; Colombini, M.P.; Marini, R.B.; Matteini, M.; Migneco, L.M.; Montenero, A.; Nodari, L.; Piccioli, C.; Zappalà, M.P.; et al. *Chimica per L'arte*; Zanichelli: Bologna, Italy, 2007; ISBN 9788808068538.
60. Eppler, R.A. *Colorants for Ceramics*; John Wiley & Sons, Inc.: Hoboken, NJ, USA, 2013.
61. Paris, R.; Frontoni, R.; Galli, G.; Lalli, C. Dalla villa al casale: Attività produttive nella Villa dei Quintili. In Proceedings of the International Conference of Studies, Prato, Italy, 20–21 October 2014; pp. 195–210.

